Catalysis Today 169 (2011) 102–111

Contents lists available at ScienceDirect

Catalysis Today

journal homepage: www.elsevier.com/locate/cattod

Methane dry reforming with CO_2 on CeZr-oxide supported Ni, NiRh and NiCo catalysts prepared by sol–gel technique: Relationship between activity and coke formation

Anita Horváth[a], Györgyi Stefler[a], Olga Geszti[b], Alain Kienneman[c], Agnieszka Pietraszek[c], László Guczi[a,d,*]

[a] Institute of Isotopes, HAS, Department of Surface Chemistry and Catalysis, P.O. Box 77, H-1525 Budapest, Hungary
[b] Research Institute for Technical Physics and Materials Science of HAS, P.O. Box 49, H-1525 Budapest, Hungary
[c] LMSPC, Laboratoire de Matériaux, Surfaces et Procédés pour la Catalyse, UMR 7515 du CNRS-ECPM-ULP, 25 Rue Becquerel, 67087 Strasbourg Cedex 2, France
[d] Chemical Research Center, Institute of Nanochemistry and Catalysis, P.O. Box 17, H-1525 Budapest, Hungary

ARTICLE INFO

Article history:
Available online 28 September 2010

Keywords:
Composite catalysts
Sol–gel technique
Methane dry reforming
Removal of surface carbon
Nickel

ABSTRACT

Ni, NiRh and NiCo catalysts supported on Ce–Zr-oxide synthesised by pseudo sol–gel method have been investigated. Monometallic samples were performed with two different Ce/Zr ratios and by conventional impregnation. BET, XPS, TPR, TPO and TEM were applied for sample characterization and dry reforming of methane was carried out with a feed mixture consisted of $CH_4/CO_2/Ar = 10/10/80$ or $CH_4/CO_2 = 70/30$ ratio. Co and Rh containing samples were proved to be stable catalysts, the impregnated Ni catalyst only slightly, while sol–gel Ni samples slowly deactivated during the long term overnight run.

The amount of carbon on the sample's surface after catalytic runs varied between 1 and 12 mg C/100 mg of catalyst. The Ni samples prepared by sol–gel and impregnation method had a peak maximum in TPO at 400 °C and 600 °C, respectively. In the case of bimetallic sol–gel samples the carbon that gave TPO peak at 360 °C was slowly transformed to that at 600 °C, showing that after several carbon deposition (dry reforming) and gasification (TPO) cycles structural changes in the catalyst and in the carbon morphology take place and graphitic carbon and nanotube formation become prevailing as was detected by TEM.

Upon high temperature pre-treatment and methane dry reforming reaction, alloyed NiRh, NiCo particles and sintered Ni were observed, with the simultaneous presence of carbidic carbon, carbon nanotubes and shell-type graphitic carbon deposition. Support degradation and segregation happened to some extent, but still there was a certain amount of Ni in strong interaction with the support probably still included in the oxide matrix. Broad metal particle size distribution seems to play a role in long term stability.

When pure methane was decomposed on Ni catalyst prepared by sol–gel method, the carbonaceous deposit could completely be removed by the subsequent CO_2 treatment, emphasizing the active role of Ce–Zr mixed oxide support in gasification of surface coke.

1. Introduction

In methane dry reforming using CO_2 ($CH_4 + CO_2 \leftrightarrow 2CO + 2H_2$) the presence of carbonaceous deposits is almost inevitable what might lead to structural degradation, deactivation and reactor plug-in in long term runs. Coke formation originates from the contribution of the different side reactions such as Boudouard reaction ($2CO \leftrightarrow CO_2 + C$) and methane decomposition reaction ($CH_4 \leftrightarrow 2H_2 + C$).

There are 2 approaches to avoid or decrease the substantial carbon formation: the first is to choose appropriate support and the second one is to modify the most frequently used nickel metal with a second one. In our previous paper [1] we have studied the behaviour of nickel catalyst supported on $MgAl_2O_4$ spinel. It was established that three different types of carbon are formed, such as: Ni-carbide, graphite and carbon nanotubes and it was proved that the crystallized carbon nanotubes are mainly responsible for the decrease in catalyst activity. The addition of small amount of gold decreased the deactivation process to some extent.

Ceria and zirconia seem to be promising supports for methane dry reforming. Darujati et al. [2] studied ceria-promoted and non-promoted $Mo_2C/\gamma\text{-}Al_2O_3$ (3 wt.% Ce, 30 wt.% Mo) catalyst and found that the ceria-promoted one had significantly higher dispersion.

* Corresponding author at: Institute od Isotopes, Konkoly Th. M. út 29/33, 1121 Budapest, Hungary.
E-mail address: guczi@mail.kfki.hu (L. Guczi).

0920-5861/$ – see front matter © 2010 Published by Elsevier B.V.
doi:10.1016/j.cattod.2010.08.004

Table 1
The major parameters of the various samples.

Catalysts	Abbreviation	Ni nominal wt.(%)	Me nominal wt.(%)	BET surf. area (m^2/g)	Lattice parameter (Å)	Support particle size (nm)
$5\%Ni/Ce_2Zr_2O_8$	Ni/Ce_2Zr_2 (imp)	5	–	17	5.27	6
$Ce_{0.6}Zr_{2.97}Ni_{0.43}O_{8-\delta}$	$NiCe_{0.6}$ $Zr_{2.97}$ (sg)	5	–	15	5.17	7
$Ce_2Zr_{1.51}Ni_{0.49}Co_{0.29}O_{8-\delta}$	NiC ◦$Ce_2Zr_{1.51}$ (sg)	3	2	11	5.30	7
$Ce_2Zr_{1.51}Ni_{0.49}Rh_{0.03}O_{8-\delta}$	$NiRhCe_2Zr_{1.51}$ (sg)	4.5	0.5	21	5.30	6
$Ce_2Zr_{1.5}Ni_{0.5}O_{8-\delta}$	$NiCe_2Zr_{1.51}$ (sg)	5	–	18	5.29	7

The catalyst provided much higher reforming activity and excellent resistance against carbon deposition compared to e.g. Ni/Al_2O_3. These enhancements are due to the fact that CH_4 and CO_2 activation occurred on both ceria and Mo_2C particles, with carbidic carbon extraction by oxygen on ceria, emphasizing the unique redox property of high surface area CeO_2. Ceria has been used not only as a modifying agent of the support, but in the form of a composite catalyst. The activity of $13.5Ni\text{-}2K/10CeO_2\text{–}Al_2O_3$ catalyst has been tested in dry reforming of methane [3]. Results suggested that both CH_4 cracking and CO disproportionation contribute to coke deposition.

The main effect of ZrO_2 is quite similar to that of CeO_2: it causes higher stability due to the strong inhibition of the carbon formation [4]. For example, addition of ZrO_2 to Ni/Al_2O_3 catalyst increased its resistance against coke formation. Through the sequential impregnation of Ni and ZrO_2 precursors Ni is supposed to be positioned close to the ZrO_2, where oxygen intermediates are dissociated and better react with carbon species [5].

The simultaneous presence of Zr and Ce-oxides is also beneficial. Rezaei et al. synthesized high surface area mesoporous nanocrystalline zirconia with pure tetragonal crystalline phase and doped with 3% Ce phase to produce excellent support for nickel catalysts in methane dry reforming [6–8]. $NiCoMgCeO_x$/zirconia–hafnia catalyst with unusually high thermal stability was applied by Choudary et al. [9].

One has to note that methane dry reforming test reactions are usually carried out with diluted reactants and so they are far from the realistic conditions. There are a few examples in the literature reporting methane dry reforming on Ce–Zr-oxides without any diluting gas. We ought to cite here the work of Corthals et al., who applied $MgAl_2O_4$ supported Ni catalysts promoted with both CeO_2 and ZrO_2 for dry reforming of methane in CH_4:CO_2 = 1:1 gas mixture without reagent dilution. It was shown that within a certain composition range, crystalline $Ce_xZr_{1-x}O_2$ mixed oxide phase was formed on $MgAl_2O_4$ that improved catalyst stability, Ni reducibility and suppressed coke formation [10]. Daza et al. investigated Ce-promoted Ni/Mg–Al samples derived from hydrotalcites [11]. They concluded that Ce promotes the reduction of Ni, acidic support favours the growth of carbonaceous deposits and basic character facilitates carbon gasification. Under "drastic conditions" their catalyst was stable up to 20 h with CH_4/CO_2 20/20 at 48 L g^{-1} h^{-1} or up to 15 h with CH_4/CO_2 40/40 at 96 L g^{-1} h^{-1}. Filamentous coke formation was demonstrated on the catalyst when gas dilution in the reactants was not used [12].

With excess amount of methane (CH_4/CO_2 = 2) Montoya et al. studied $Ni/ZrO_2\text{–}CeO_2$ sol–gel catalysts for dry reforming of methane, and declared that phase transformation, support sintering and not coke formation was the main cause of the deactivation. Solid solution of $CeO_2\text{–}ZrO_2$ was formed by adding 1, 8, 20% CeO_2 to $15\%Ni/ZrO_2$. It was stated that Ce-oxide prevented the tetragonal to monoclinic transformation of ZrO_2 and the part of Ni^{2+} was incorporated in ZrO_2, and CeO_2 being partially segregated in the case of 20% CeO_2 [13].

The aim of this paper is to study the Ce–Zr-oxide based metal catalysts prepared by sol–gel technique or impregnation method to gather information about their structure, activity and the different carbonaceous species formed during CH_4 dry reforming with CO_2. It is well known that natural methane source sometimes contains about 30 vol.% CO_2. For this reason we apply a gas mixture composed of CH_4/CO_2 = 70/30 ratio without any dilution by which coke formation is of high chance.

2. Experimental

2.1. Catalyst preparation

The monometallic Ni and bimetallic NiRh and NiCo catalysts were prepared by pseudo sol–gel method based on thermal decomposition of metallic propionates [14,15]. The metal precursors used for synthesis were: cerium (III) acetate sesquihydrate, zirconium (IV) acetylacetonate, rhodium (II) acetate dimer, nickel (II) acetate hydrate and cobalt (II) acetate hydrate. The salts were dissolved in the excess of propionic acid and the solutions were mixed and heated under reflux. The solvent was evaporated to obtain gel which was than calcined in air at 750 °C during 4 h. Monometallic Ni samples were prepared with two different Ce/Zr ratio $Ce_{0.6}Zr_{2.97}$ and $Ce_2Zr_{1.5}$, respectively (named as $NiCe_{0.6}Zr_{2.97}$ (sg) and $NiCe_2Zr_{1.51}$ (sg)), the latter composition was further set for the preparation of NiRh and NiCo catalysts (denoted as $NiRhCe_2Zr_{1.51}$ (sg) and $NiCoCe_2Zr_{1.51}$ (sg)) (Table 1).

The reference Ni/Ce_2Zr_2 (imp) catalyst was prepared by wet impregnation of $Ce_2Zr_2O_8$ support, prepared by previously mentioned sol–gel technique, in excess of water which was then removed during heating up to 160 °C under stirring. The obtained residue was dried overnight and calcined in air at 750 °C during 4 h. The metal precursor used in this case was nickel (II) nitrate hexahydrate. The nominal metal concentrations of the samples are shown in Table 1. It has to be stressed here that metal loading for all the catalysts is always the same, equal to 5 wt.%.

2.2. Sample characterization

The specific BET surface area was determined by N_2 adsorption–desorption measurements at −196 °C in a Tristar gas adsorption system. The crystalline structure of mixed oxides was determined by powder X-ray diffraction using Brucker D8 Advanced apparatus with CuKα radiation. The lattice parameters, support particle sizes and BET specific surface areas are summarized in Table 1.

The reducibility of selected catalysts was studied by temperature programmed reduction (TPR) using 0.05 g sample heated from room temperature to 900 °C with a ramp of 15 °C/min under hydrogen/argon flow.

The oxidation state and surface concentration of Ni on $NiCe_{0.6}Zr_{2.97}$ (sg) were determined by XPS performed by a KRATOS XSAM 800 XPS machine equipped with an atmospheric reaction chamber. Spectra were taken in (a) the "as prepared" form of the sample and after each in situ subsequent treatment; (b) flowing H_2 at 770 °C; (c) reaction mixture of CH_4/CO_2 = 70/30 at 660 °C; (d) air at 700 °C and (e) again reaction mixture at 660 °C. AlK_α excitation and 40 eV pass energy was used during data acquisition. The binding energies (BE) were determined relative to C 1s at 285 eV.

For the surface composition, signals of Ni 2p, Ce 3d, Zr 3d, O 1s, and C 1s were considered using the sensitivity factors given by the manufacturer. In fitting the entire Ni 2p region first a Shirley-type background was subtracted The entire Ni 2p region was fitted using 17.3 eV separation between the $2p_{1/2}$ and $2p_{3/2}$ states and 6 to 7 eV separation for the satellites of the Ni^{2+} peaks.

The amount of carbon on the sample surface after catalytic run with CH_4/CO_2 = 70/30 feed was estimated from the amount of CO_2 evolved in TPO experiments carried out in 5 vol.% O_2 and 1 vol.% Ar in He. To detect CO_2 formation mass spectrometer was employed. Using the correlation between the intensity and flow ratio of CO_2 to Ar the flow of CO_2 could be determined and then integrated through the time, which resulted in the amount of CO_2 formed [1].

The Ni particle size and the structure of the carbon species were studied by a Philips CM20 TEM operating at 200 kV equipped with a NORAN energy dispersive spectrometer (EDS) of germanium detector for electron probe microanalysis. The aqueous suspensions of the samples were dropped on carbon-coated grid and after evaporating water the electron micrographs of the particles were taken.

2.3. Catalytic activity

Catalytic tests were performed under two different conditions in fixed bed quartz reactors. The first set of activity measurements was performed on 0.1 g of catalyst with a feed mixture consisted of $CH_4/CO_2/Ar$ = 10/10/80 and total space velocity of 30 L h^{-1} g^{-1}. Prior to the reaction the catalyst was reduced in 5% H_2–95%Ar at 750 °C for 4 h (0.0025 L/min). The reforming activity was studied increasing the temperature from 550 °C to 800 °C with the stabilization of 2 h at each temperature.

A second set of catalytic reaction was performed using CH_4/CO_2 = 70/30 mixture without any diluting inert gas to mimic realistic reforming gas composition. 0.1 g of catalyst was put into the quartz reactor and the reactant mixture with 20 ml/min flow rate (total space velocity 12 L/gh) was introduced after the standard reduction pre-treatment that means 100% H_2 at 750 °C for 4 h. Temperature during the reaction was raised up to about 800 °C until all the CO_2 was consumed (standard reaction with temperature ramp). When repeated reactions were carried out, the reduction treatment at 750 °C took only 1 h after TPO (that served as calcination as well). A quadrupole mass spectrometer (type Balzers 100) was used for analysis of the reaction products and the methane and carbon dioxide conversions were calculated [1].

Long term (overnight) stability tests using CH_4/CO_2 = 70/30 mixture were carried out in he following way. First, a standard reaction with temperature ramp up to 750–800 °C was conducted on fresh, calcined and reduced sample, then the system was cooled down to 650 °C in $CO_2 + CH_4$ mixture and the stability measurement was started at that point and lasted for about 24 h. During the stability tests the main stream of the effluent gas mixture was connected to a gas chromatograph Chrompack 900 and CO, CO_2 and CH_4 were separated on a 5 m long 60/80 Carboxen 1000 column.

3. Results and discussion

The XRD patterns (Fig. 1(a)–(e)) are shown for Ni/Ce_2Zr_2 (imp), $NiCe_{0.6}Zr_{2.97}$ (sg), $NiCe_2Zr_{1.51}$ (sg), $NiRhCe_2Zr_{1.51}$ (sg) and $NiCoCe_2Zr_{1.51}$ (sg) catalysts after calcination in air at 750 °C for 4 h. It can be clearly seen that the patterns match well to the face-centered cubic structure of $Ce_{0.6}Zr_{0.4}O_2$ (JCPDS 38-1439). Nevertheless, the small, broad peaks at $2\theta = 37.3°$ and 43.3° indexed as NiO, with (0 0 1) and (2 0 0) planes can also be observed for all samples except $NiCe_{0.6}Zr_{2.97}$ (sg) one even after zoom in this region. We suggest that this difference for NiCeZr (sg) catalysts is due to to the varying Ce/Zr ratio. It might be explained by partial rejection

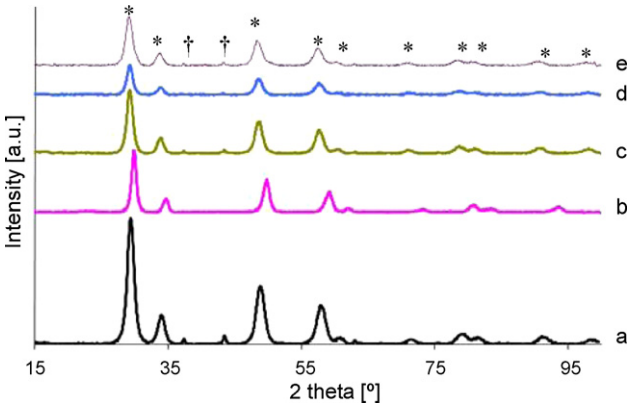

Fig. 1. XRD of freshly prepared catalyst: (a) Ni/Ce_2Zr_2 (imp); (b) $NiCe_{0.6}Zr_{2.97}$ (sg); (c) $NiCoCe_2Zr_{1.51}$ (sg); (d) $NiRhCe_2Zr_{1.51}$ (sg); (e) $NiCe_2Zr_{1.51}$ (sg). * face-centered cubic fluorite structure, † NiO species.

of Ni from the host Ce–Zr structure. For the bimetallic catalysts besides diffraction patterns characteristic of fluorite structure and NiO species, no evidence of Co or Rh oxides was observed. In the case of Rh-containing catalyst this could be ascribed to the low Rh loading (~0.5 wt. %). In the all cases total metal loading was 5 wt.% and it was demonstrated that not all the metal can be inserted into host Ce–Zr fluorite structure. For $NiCoCe_2Zr_{1.51}$ (sg) catalyst it is nickel, which is rejected due to the difference in ionic radii of Co^{2+} (75pm), Ni^{2+} (69 pm) and Zr^{4+} (84 pm). Co^{2+} ionic radius is more compatible with Zr^{4+} one than the Ni^{2+}. It was also stated that the insertion of Ni up to 3 wt.% into fluorite Ce–Zr structure do not lead to the rejection [16].

The catalytic tests demonstrate the temperature dependence of catalytic activity in diluted reactant feed (Fig. 2) and in pure $CH_4 + CO_2$ mixture (Figs. 3 and 4). It should be noted that CH_4 conversion was always lower than CO_2 one. This phenomenon is particularly remarkable with the CH_4/CO_2 = 70/30 composition. It is due to the presence of reverse water gas-shift reaction (RWGS: $CO_2 + H_2 \leftrightarrow H_2O + CO$) occurring simultaneously with CO_2 reforming of CH_4 [17]. In the case of $CH_4/CO_2/Ar$ = 10/10/80 the highest CO_2 and CH_4 conversion was observed for $NiRhCe_2Zr_{1.51}$ (sg) sample, Ni/Ce_2Zr_2 (imp) catalyst exhibited quite similar activity while the monometallic $NiCe_{0.6}Zr_{2.97}$ (sg) had the lowest activity. This activity order changed in non-diluted gas mixture proving that

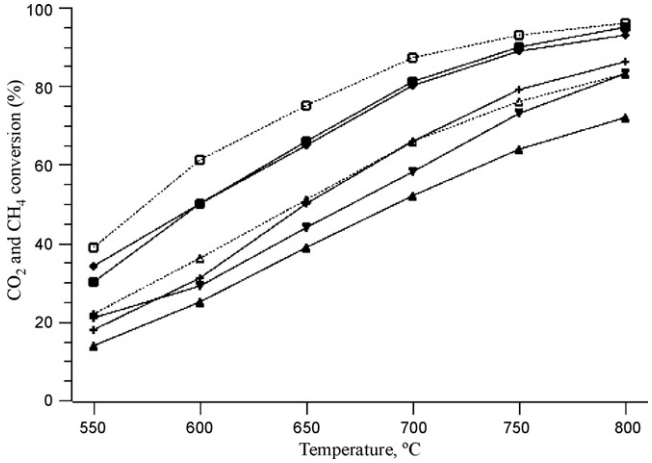

Fig. 2. Dry reforming tests with diluted reactants. CH4 conversions for (♦) Ni/Ce_2Zr_2 (imp); (+) $NiCoCe_2Zr_{1.51}$ (sg); (▲) $NiCe_{0.6}Zr_{2.97}$ (s/g), (···) $NiCe_2Zr_{1.51}$ (sg) and (■) $NiRhCe_2Zr_{1.51}$ (sg). CO_2 conversions are depicted with dotted lines for the most and the least active samples: (□) $NiRhCe_2Zr_{1.51}$ and (Δ) $NiCe_{0.6}Zr_{2.97}$ (sg). Reaction conditions: $CH_4/CO_2/Ar$ = 10/10/80; total space velocity: 30 L h^{-1} g^{-1}.

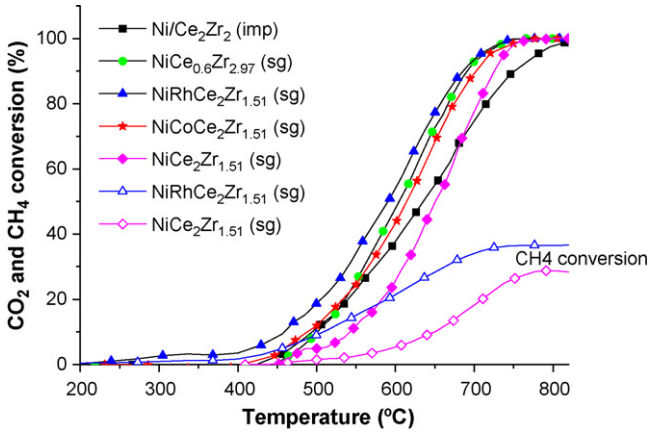

Fig. 3. Comparison of CO_2 conversion curves (and CH_4 conversion of the most and least active samples) in the first reaction after reduction treatment at 750 °C/4 h. Reaction conditions: CH_4/CO_2=70/30; total space velocity: 12 L h^{-1} g^{-1}; temperature ramp 10 °C/min.

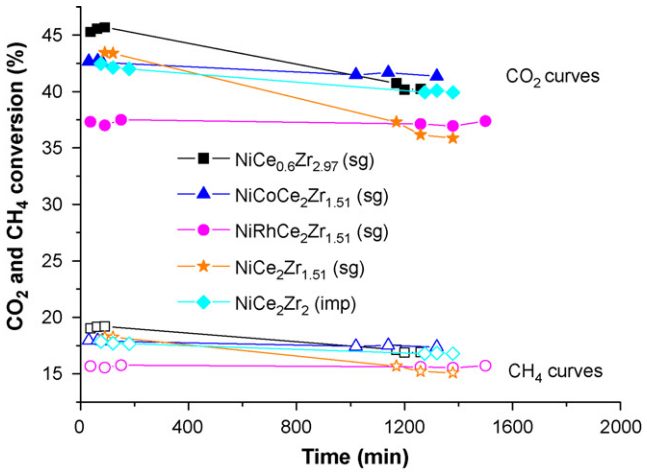

Fig. 5. Long term stability tests at 650 °C on "spent" samples. Reaction conditions: CH_4/CO_2 = 70/30; total space velocity: 12 L h^{-1} g^{-1}.

reaction conditions may influence the overall catalytic behaviour to a great extent and that the comparison of catalyst samples without giving the reaction details can be misleading.

For the results obtained in the CH_4/CO_2 = 70/30 mixture the most active sample was again $NiRhCe_2Zr_{1.51}$ (sg) catalyst, the second one was $NiCe_{0.6}Zr_{2.97}$ (sg), while $NiCe_2Zr_{1.51}$ (sg) sample proved to be the worst catalyst, although the difference between the conversions vs. temperature curves is small (see Fig. 3). There is a slight deviation in the rise of curve obtained for Ni/Ce_2Zr_2 (imp) suggesting different catalyst structure. Fig. 4 depicts the effectiveness of several reaction-regeneration cycles on the CO_2 conversion values of $NiRhCe_2Zr_{1.51}$ (sg) sample. It is clearly seen that the original activity can be regained by calcinations (TPO)/reduction cycles. Note that the curve is the same if only TPO not followed by reduction was applied to remove the carbonaceous contamination, meaning that the Rh containing sample is able to get reduced by the gas mixture present. The same applies for the other samples, although there is a sudden jump in the conversion values as the temperature reaches the sufficient 620 °C (results not shown here) suggesting that reduced state of Ni is needed for high catalytic activity.

The stability of catalysts in the CH_4/CO_2 = 70/30 mixture in overnight reaction at 650 °C was also measured as shown in Fig. 5. Note that these tests were carried out on catalyst samples previously used in a standard reaction with temperature ramp (spent samples), that means carbonaceous contamination formed up to 750–800 °C were already present on their surface. Thus, we should handle the starting points in Fig. 5 as data of a kind of second reaction without any regeneration. Co and Rh containing samples seem to be stable catalysts, the impregnated Ni catalyst only slightly, while sol–gel monometallic Ni samples slowly but surely deactivate during 24 h. The addition of 0.5 wt.% Rh apparently prevents the long term deactivation during overnight test. However, according to Fig. 5 and Fig. 3, the $NiRhCe_2Zr_{1.51}$ (sg) sample shows the largest activity decrease after a standard reaction with temperature ramp, since the CO_2 conversion in Fig. 5 is only 48% compared to the conversion value of the fresh, calcined and reduced sample (corresponding data point at 650 °C in Fig. 3). Thus, we can declare that the Rh-containing sol–gel sample besides the high activity has a high tendency for fast, initial deactivation but then stable activity is maintained for even 24 h. Addition of Co turns to be more favourable, since the presence of Co also improves catalyst stability but provides higher CO_2 and CH_4 conversion after 24 h than the Ni, Rh sol–gel sample. However, we should keep in mind that Co content is 2 wt.% compared to the 0.5 wt.% Rh content of $NiRhCe_2Zr_{1.51}$ (sg). Studies on Ni and Co-containing perovskite-type oxide catalysts revealed the synergetic effect of Ni and Co contributing to catalyst stability [18,19], while other work showed that cobalt decreased the methane reforming activity of Ni [20].

We can conclude that our catalytic test reactions proved the beneficial effect of 0.5 wt.% Rh and 2 wt.% Co on catalyst stability, while, as for the sol–gel Ni samples, the higher Zr content in the mixed oxide support resulted in a more active but still deactivating catalyst. It is interesting to note the relatively good catalytic performance of the impregnated Ni catalyst.

One possible reason of decreasing activity of the catalyst is the coke formation that gradually blocks catalyst active sites for methane dry reforming reaction. In order to study the surface carbonaceous deposits formed during the reaction in CH_4/CO_2 = 70/30 mixture, temperature programmed oxidation (TPO) of the surface carbon was performed. The T_{max} obtained in TPO curves may be characteristic of the carbon bond strength to the catalyst surface, reflects the kinetics of carbon burning process, while the CO_2 amount evolved during the oxidation enables quantitative comparison. The results obtained are summarized in Fig. 6(a)–(e). $NiCe_{0.6}Zr_{2.97}$ (sg), $NiCe_2Zr_{1.51}$ (sg) (Fig. 6(a),(b)) and $NiCoCe_2Zr_{1.51}$ (sg) (Fig. 6(d)) samples were the least contaminated (1–3 mg C/100 mg catalyst depending on the conditions prior to TPO), $NiRhCe_2Zr_{1.51}$ (sg) (Fig. 6(e)) had a medium amount of sur-

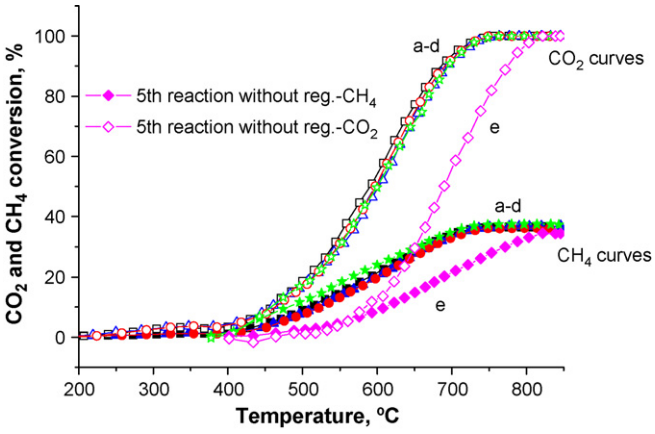

Fig. 4. Catalytic activity of $NiRhCe_2Zr_{1.51}$ (sg) sample in subsequent reactions: (a) 1st reaction; (b) 2nd reaction after TPO/reduction (regeneration); (c) 3rd reaction after regeneration; (d) 4th reaction after TPO only and (e) 5th reaction without regeneration. Reaction conditions: CH_4/CO_2 = 70/30; total space velocity: 12 L h^{-1} g^{-1}, temperature ramp 10 °C/min.

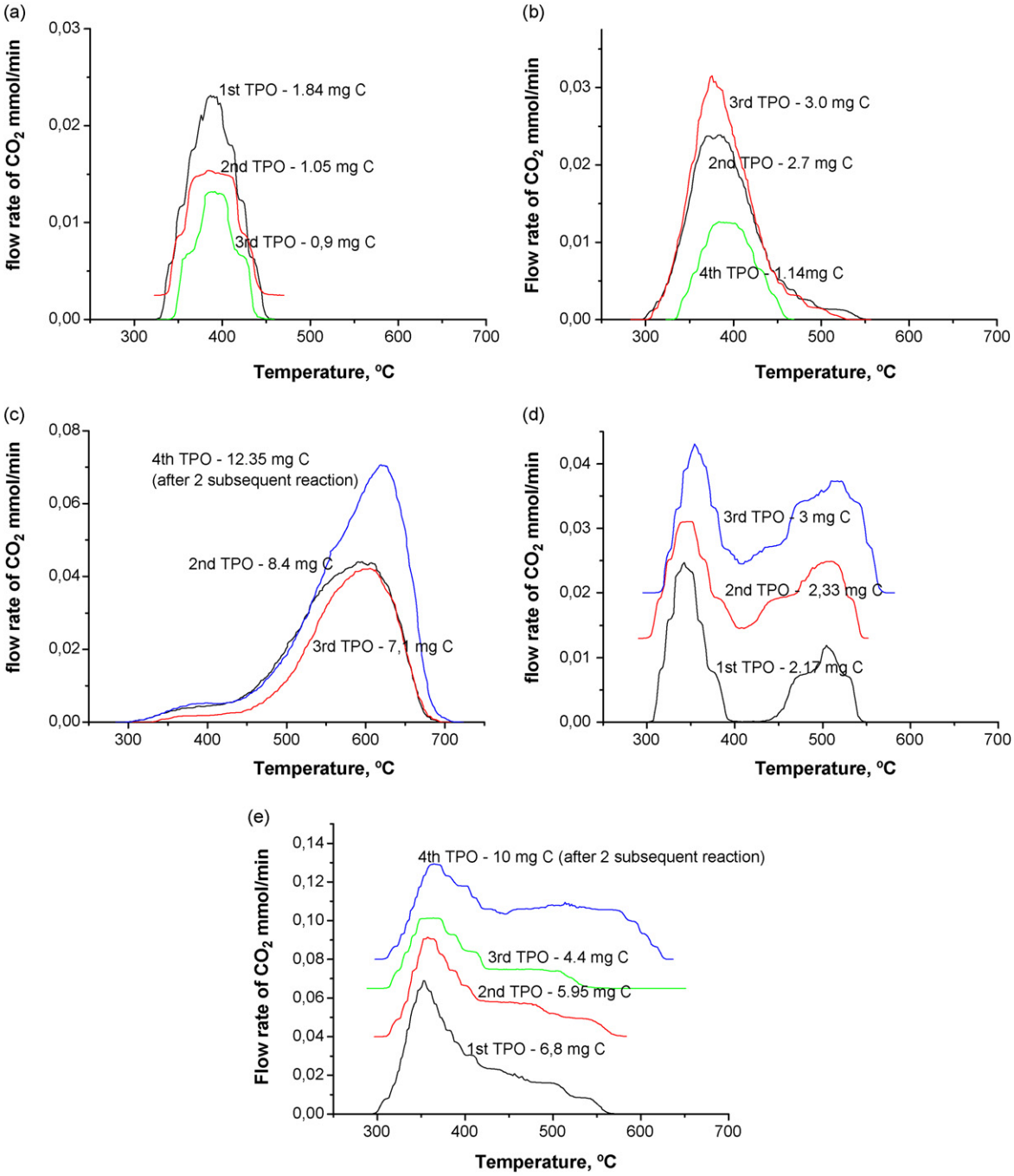

Fig. 6. TPO measurements on: (a) $NiCe_{0.6}Zr_{2.97}$ (sg); (b) $NiCe_2Zr_{1.51}$ (sg); (c) Ni/Ce2Zr2 (imp); (d) $NiCoCe_2Zr_{1.51}$ (sg) and (e) $NiRhCe_2Zr_{1.51}$ (sg). Before each TPO a catalytic reaction with temperature ramp was conducted on the regenerated sample. In some cases curves are shifted for the sake of clarity.

face carbon of 4–10 mg while the highest amount of carbon was retained by the surface of 5% Ni impregnated on Ce_2Zr_2-oxide support (7–12 mg C) (Fig. 6(c)). The results reflect that there is no straightforward relation between catalytic activity and the amount of surface carbon measured. Comparing the amount of CO_2 produced during the TPO with that obtained on 8.8% $Ni/MgAl_2O_4$ [1] on which the surface carbon was significantly higher, we ascertain the significant role of Zr–Ce mixed oxide in the gasification of surface carbon by reverse Boudouard reaction ($C + CO_2 = 2CO$) or $C + H_2O$ reaction to form $CO + H_2$.

The Ni samples produced CO_2 in a single peak but with 200 °C of difference depending on the preparation method: sol–gel samples had a peak maximum at 400 °C, while the position of TPO peak maxima was shifted to 600 °C for the impregnated catalyst (however, note the small shoulder at 400 °C). In the case of bimetallic sol–gel samples the low and the high temperature peak was simultaneously observed but each one shifted to lower values, to 350 °C and about 500 °C. Furthermore, the ratio between low and high temperature peaks apparently changed which points to the alteration of catalyst/carbon structure after repeated reactions and changes with the nature of the second metal. In the case of $NiRhCe_2Zr_{1.51}$ (sg) catalyst less high temperature carbon was observed.

Close investigation of TPO data reveals that the amount of carbon slightly decreases on spent samples (see 1st, 2nd and 3rd TPO data). We also observed that the amount of carbon after the overnight reaction is sometimes lower than in a single reaction

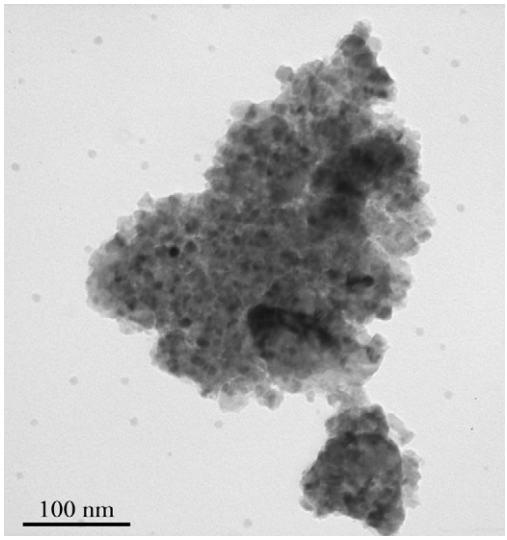

Fig. 7. TEM image of $NiCe_2Zr_{1.51}$ (sg) in as prepared (calcined) state.

with temperature ramp in agreement with Verykios co-workers who detected decreased amount of carbon on Rh/Al_2O_3 after 2 h of reaction [21,22]. This observation also suggests a structural change in the catalyst and carbon morphology as well while repeating the carbon deposition (dry reforming) and gasification (TPO) cycles. Goula et al. studied the coking behaviour of $Ni/CaO–Al_2O_3$ catalyst in dry reforming and found that the rates of carbon formation and removal depends on time on stream and catalyst surface composition (the amount of carbon increased or decreased after 15 min time on stream depending on the catalyst) [23]. Chen et al. also detected that cyclic carbon formation–gasification reduced the filamentous carbon formation [21].

Transmission electron microscopy (TEM) images (Figs. 7–10 and 12) of the catalyst samples support the observation performed by TPO. In the as prepared state of the sol–gel samples

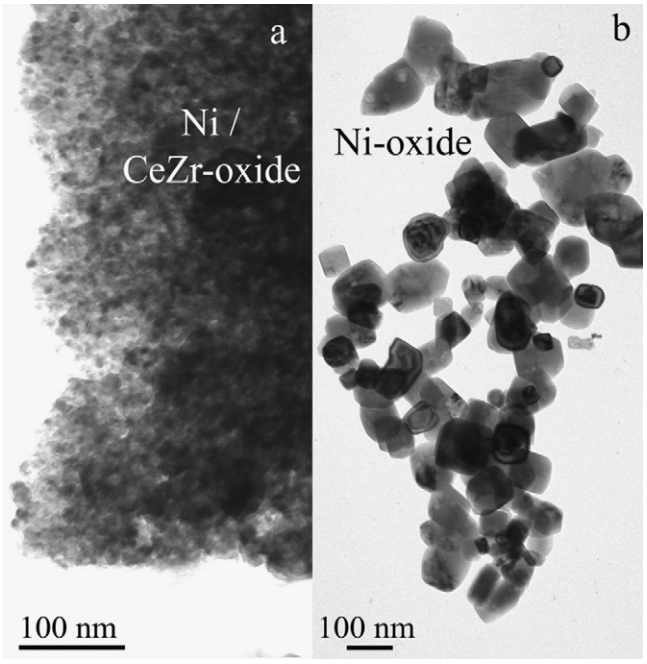

Fig. 8. TEM images of Ni/Ce_2Zr_2 (imp) in as prepared state: (a) support with Ni-oxide nanoparticles incorporated and (b) separated Ni-oxide particles detached from the support.

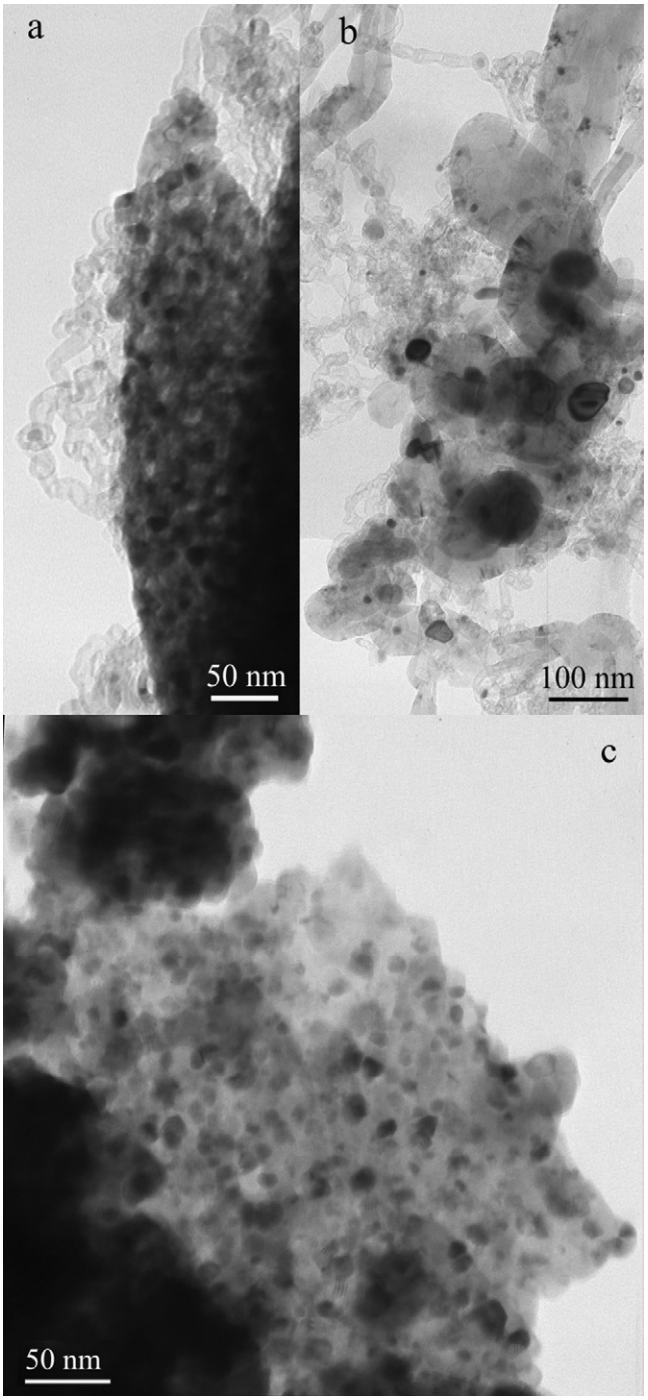

Fig. 9. TEM images of Ni sol–gel samples after long term test: (a) small Ni particles of $NiCe_{0.6}Zr_{2.97}$ (sg) incorporated in the support and inside thin nanotubes and (b) sintered Ni particles of $NiCe_{0.6}Zr_{2.97}$ (sg) separated from the support, encapsulated in carbon and thick nanotubes; (c) no sign of filamentous carbon on $NiCe_2Zr_{1.51}$ (sg). (Conditions: overnight reaction at 650 °C in CH_4/CO_2 = 70/30; total space velocity: 12 L h^{-1} g^{-1}).

after initial calcination nickel and the other metals are intimately incorporated in a solid Ce–Zr-oxide composite material which is rather compact, and sign of larger metal-oxide particles is hardly seen. The size of the nickel-oxide particles could be rarely distinguished by TEM remained in nano range between 4 and 6 nm. Fig. 7 shows the TEM image of $NiCe_2Zr_{1.51}$ (sg) in as prepared state as a representative example. In the case of the impregnated sample probably due to the weak interaction between the Ni-nitrate precursor and the support, 2 types of Ni-oxide species

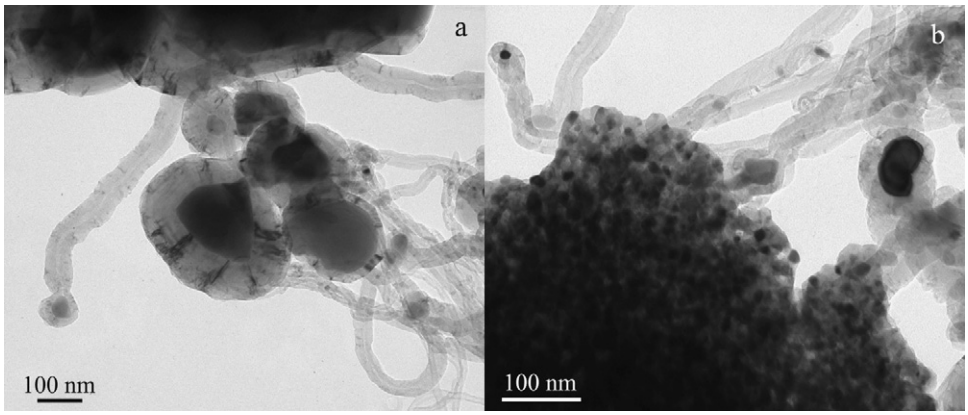

Fig. 10. TEM images of Ni/Ce_2Zr_2 (imp) after long term test: (a) Ni particles of 100–300 nm surrounded by graphitic shell and separated from the support and (b) support with smaller Ni particles inside carbon nanotubes (Conditions: overnight reaction at 650 °C in CH_4/CO_2 = 70/30; total space velocity: 12 L h^{-1} g^{-1}).

were detected: Ni-oxide that is incorporated in the oxide matrix (Fig. 8a), and agglomerated 50–150 nm large Ni-oxide particles detached from the support surface (Fig. 8b). As for the bimetallic samples, Co is seen by EDS analysis, while the amount of Rh seen by EDS technique was only slightly above the detection limit.

Significant changes can be observed in the structure of all samples after the catalytic reactions that include high temperature oxidation/reduction treatments as well. By comparison of $NiCe_{0.6}Zr_{2.97}$ (sg) and $NiCe_2Zr_{1.51}$ (sg) after overnight reaction (Fig. 9(a)–(c), respectively), TEM images clearly indicate that catalyst with higher Ce/Zr ratio does not produce filamentous carbon. Moreover, the electron diffraction (SAED not shown here) detected Ni in oxidic form in the case of $NiCe_2Zr_{1.51}$ (sg). According to Fig. 9(a) and (b), $NiCe_{0.6}Zr_{2.97}$ (sg) contains a certain amount of Ni that is in strong interaction with the support probably still included in the oxide matrix, while there are Ni particles of 5–80 nm inside carbon nanotubes and encapsulated by graphitic layers separated from the parent mixed oxide support. In this case SAED (selected area electron diffraction) pattern showed the presence of Ni-carbide and metallic Ni. Junke et al. observed suppressed formation of filamentous carbon when the diameter of metal particles was smaller than 15 nm [24]. This and the oxidized state of nickel probably caused by higher amount of Ce in the support might be the reason for the lack of nanotubes.

The surface carbon of these samples can be easily removed by O_2 (see the corresponding TPO curves in Fig. 6). Since $NiCe_2Zr_{1.51}$ (sg) is less active and less stable in reforming reaction even with no filamentous carbon formation, its poorer catalytic performance should be more attributed to the partial re-oxidation of nickel particles than to the carbon formation.

The impregnated Ni sample produced the highest amount of coke: carbon nanotubes of different diameters and encapsulating type carbon were seen after the reforming reaction (see Fig. 10(a) and (b)). The kinetics of carbon filament formation is well described in the literature, depending on the conditions (depending on the rate of carbon nucleation and rate of carbon diffusion): pear shaped Ni appears at high temperature with hollow filaments, conical shaped Ni and full filaments at lower temperature [25] while fragmentation of the metal particle due to its destruction by the growing carbon filament can also happen [26]. We also observed differently shaped Ni particles inside the nanotubes and Ni particles of more than 200–300 nm surrounded by graphitic shell of about 80 nm thickness (see Fig. 10(a)). Those were produced from the agglomerated Ni-oxide particles already seen in as prepared state. Despite the very broad size distribution of this sample the catalytic stability is considerably higher than that of the sol–gel Ni samples, suggesting that large particles must be involved in the maintenance of long term activity.

Now we consider the results of TPR (Fig. 11(a)–(c)) on $NiCe_{0.6}Zr_{2.97}$ (sg), $NiCe_2Zr_{1.51}$ (sg) and Ni/Ce_2Zr_2 (imp) samples. The TPR profiles are composed of two peaks totally different for sol–gel and impregnated catalysts. This is due to the presence or lack of strong metal support interaction. The impregnated Ni sample (Fig. 11b) is reduced at lower temperature. The hydrogen consumption at ca. 310–320 °C is assigned to Ni particles free of interaction and the peak at 380–420 °C could correspond to nickel incorporated into the Ce–Zr structure. Peak at 380 °C indicates that even by impregnation, small part of nickel could be integrated into the fluorite. For Ce–Zr-oxide, two small peaks at 600 °C and 780 °C have been evidenced [27]. In Fig. 11(a), peak at 600 °C could be also attributed to ceria reduction helped by the presence of reduced nickel. For Ni/Ce_2Zr_2 (imp) reduction of ceria occurs more slowly between 550 °C and 730 °C. Oxygen from ceria-zirconia is more mobile, and thus more available than oxygen resulting from the impregnated catalyst. This might be in relation with the carbon removal after catalytic test where mobility of oxygen is of high importance in deposited carbon oxidation. Furthermore, the less the reduction temperature, the bigger the size of Ni particles will be (TEM).

For the bimetallic sol–gel samples, the structural degradation and support segregation after catalytic run are even more pronounced. In the case of NiC °$Ce_2Zr_{1.51}$ (sg), the EDS analysis dur-

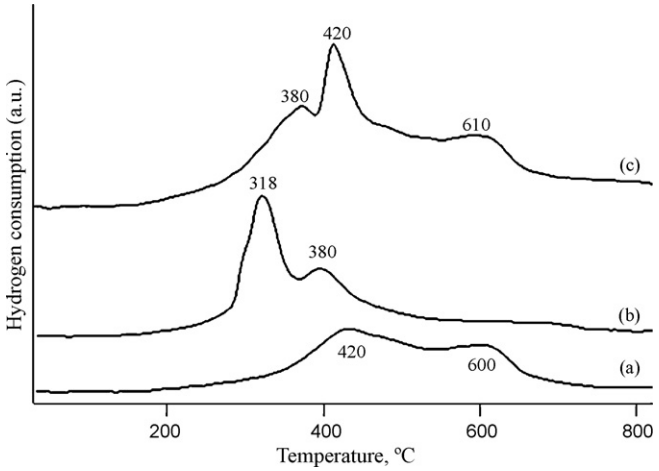

Fig. 11. TPR profiles of (a) $NiCe_{0.6}Zr_{2.97}$ (sg); (b) Ni/Ce_2Zr_2 (imp); and (c) $NiCe_2Zr_{1.51}$ (sg) catalysts.

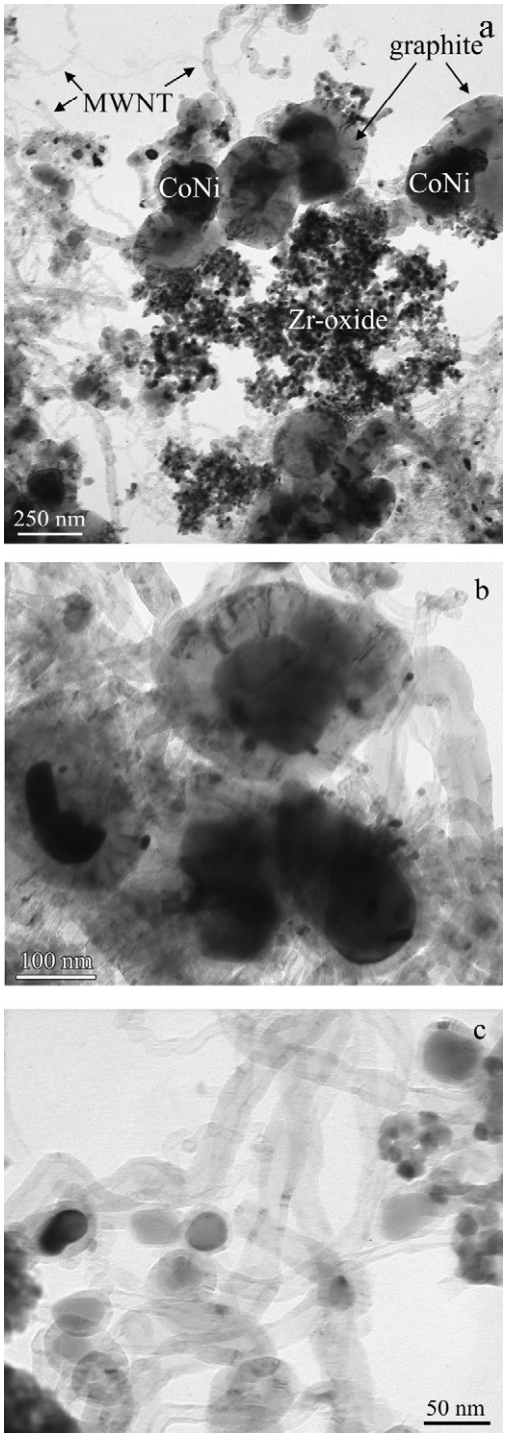

Fig. 12. TEM images of bimetallic sol–gel samples after long term test: (a) $NiCoCe_2Zr_{1.51}$ (sg); (b) large, encapsulated NiRh particles on $NiRhCe_2Zr_{1.51}$ (sg) and (c) smaller encapsulated Ni particles and carbon nanotubes on $NiRhCe_2Zr_{1.51}$ (sg). (Conditions: overnight reaction at 650 °C in CH_4/CO_2 = 70/30; total space velocity: 12 L h^{-1} g^{-1}).

ing TEM detected bimetallic 50–200 nm NiCo particles shown in Fig. 12(a) surrounded by thick encapsulating carbon together with the presence of thin nanotubes containing small Ni particles inside. Support segregation occurs to some extent as well, see the small particles in Fig. 12(a) signed as ZrO_2 which contain Ni according to EDS. Alumina supported Ni–Co bimetallic catalysts were studied in dry reforming of methane and the 7.6 wt.% Co monometallic sample was the most active one producing the largest amount of carbon deposit of encapsulating and filamentous form [28].

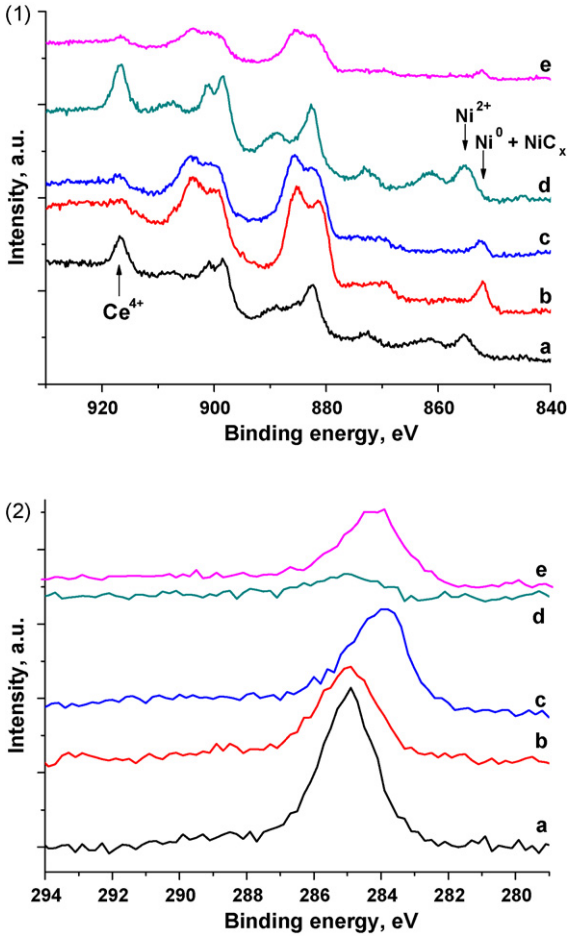

Fig. 13. (1) XPS spectra on $NiCe_{0.6}Zr_{2.97}$ (sg) sample: (a) as received, (b) after reduction in H2 at 770 °C/1 h, (c) after $CO_2 + CH_4$ reaction at 660 °C, (d) treatment in air at 700 °C/1 h and (e) after $CO_2 + CH_4$ reaction at 660 °C; (2) XPS spectra of carbon C 1s on $NiCe_{0.6}Zr_{2.97}$ (sg) sample: (a) as received, (b) after reduction in H_2 at 770 °C/1 h, (c) after $CO_2 + CH_4$ reaction at 660 °C, (d) treatment in air at 700 °C/1h and (e) after $CO_2 + CH_4$ reaction at 660 °C.

The sample $NiRhCe_2Zr_{1.51}$ (sg) looks somewhat similar to $NiC°Ce_2Zr_{1.51}$ (sg) in TEM images (Fig. 12b and c). 100–150 nm size bimetallic NiRh particles and several large Ni particles were formed and encapsulated by graphitic shell, sit in the network of filamentous carbon. The original mixed oxide phase might have been also segregated to some extent.

Considering the above observations, now we tend to describe TPO peaks obtained at high and low temperature to carbonaceous deposits of two distinctly different types in contact with distinctly different metal proximity. Pan et al. observed that for Ni/Al_2O_3 depending on the feed gas composition, ratio of encapsulating and filamentous carbon was different, and when most of the carbon was encapsulating type, the TPO peak appeared at lower temperature (under 600 °C) [29]. We suggest, when small metallic particles in strong interaction with support being able to provide active oxygen are present and carbidic, amorphous or thin fragile filamentous carbon is formed, the TPO peak appears at lower temperatures, (or as in the case of the single TPO peak of Ni sol–gel samples). When sintered metal particles detached from the support oxidize graphitic robust nanotubes or thick rather encapsulating type carbon, TPO peaks are observed around 500–600 °C. The beneficial effect of Rh and Co addition is seen in the relative ease of oxidation of any kind of coke compared to the Ni samples that manifests itself in the decrease of TPO maxima. The other positive effect of Co and Rh might be the prevention of Ni oxidation and active alloy formation resulting in stable catalytic activity in the long term test.

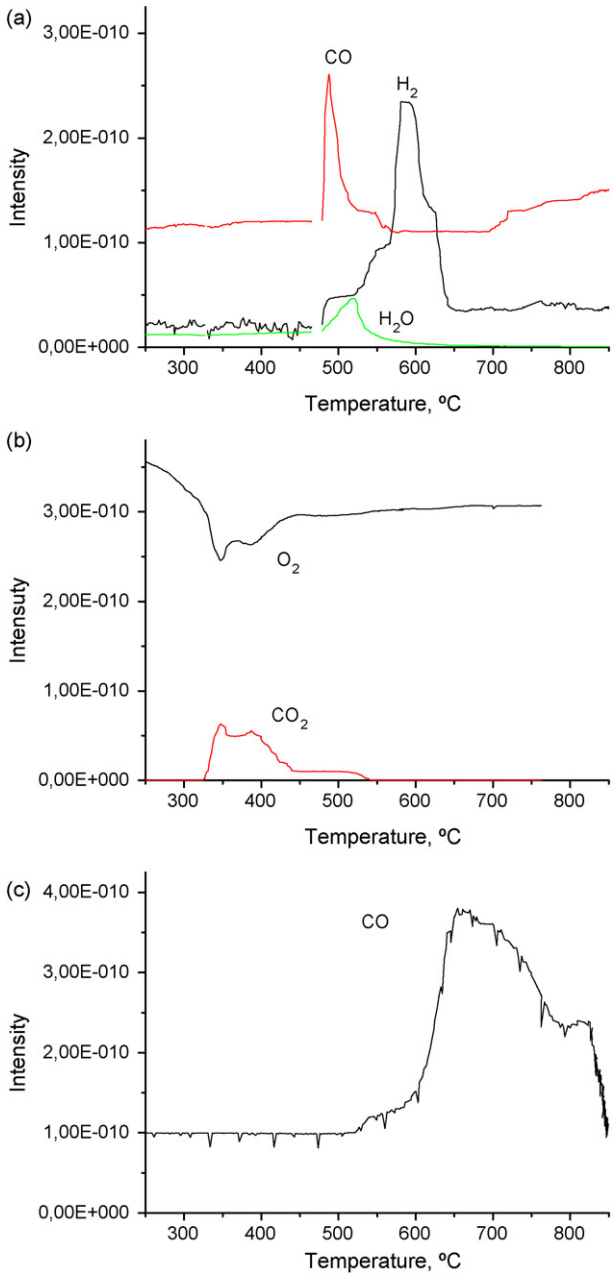

Fig. 14. (a) Temperature programmed reaction (decomposition) of CH_4 on $NiCe_{0.6}Zr_{2.97}$ (sg) that was cleaned by TPO previously; (b) after cooling down to RT the sample was treated in 10% O_2 in He and (c) after second CH_4 decomposition the sample was treated in 20%CO_2 in He to remove surface carbon.

In agreement with the literature, thus, there are several type of carbon in our catalysts, viz. amorphous and carbidic carbon, filamentous that can be nanotube with Ni particle inside and shell-like that also encapsulates Ni but it is not of filamentous form. Encapsulating carbon is declared to cause deactivation, by blocking the metal surface [30], while beside of the formation of filamentous type carbon, even with a graphitic structure, catalyst can still work [31–33]. However, if the filamentous carbon formation is accelerated, eventually it is also detrimental causing catalyst plug-in, structural and metal particle destroy. For the increased formation of nanotubes metal particles should possess proper morphology in terms of exposure of open ⟨1 0 0⟩ and ⟨1 1 0⟩ and ⟨1 1 1⟩ crystal planes at the front and the back side, thus, for any reason "smoothened" metal particles produce less filaments but more amorphous carbon and Ni_3C or at high temperature shell-like encapsulating carbon [34,35]. This can explain the reduced carbon formation on both NiCeZr (sg) samples, which do not contain large, faceted Ni, but rather small, Ni-oxide probably still incorporated in the oxide matrix.

Despite the fact that our catalyst are sintered, contaminated by all kinds of carbon, catalytic activity is extremely good concerning the reaction conditions (CH_4/CO_2 = 70/30) that are highly susceptible for coke formation. This indicates that carbon contamination may play a dynamic role in the reaction to produce CO in agreement with Ref. [3].

Alonso et al. pointed out that broad particle size is even beneficial in catalytic point of view, because small particles causes CH_4 decomposition at the beginning of methane dry reforming, while large particles are responsible for long term stability due to the formation of non deactivating carbon deposits. The $CO_2 + C = CO$ (carbon gasification) reaction is structure sensitive favoured on small particles while the filamentous carbon formation is suppressed [28]. This is in complete agreement with our results, since all the samples have broad size distribution after catalytic tests, and the samples that contain larger Ni or NiCo, NiRh particles exhibit more stable activity.

The $NiCe_{0.6}Zr_{2.97}$ (sg) sample was further investigated by X-ray photoelectron spectroscopy (XPS). In Fig. 13 (1) the change of Ni 2p + Ce 3d spectra are plotted using in situ measurements (the measurement was performed on the same sample placed into a reaction chamber attached to the XPS machine, and after each treatment the XP spectra were directly recorded). Fig. 13 (2) shows the change of C 1 s region after the various treatments. For the better identification the intensity of the spectra has been shifted. Detailed data on the surface concentrations as well as the Ni/Zr ratios and sample charging during the XPS measurement are given in Table 2.

In the "as prepared" state the nickel was in the form of Ni_2O_3 with 855.5 eV BE and the cerium in CeO_2 showing the characteristic satellite peak at 916.7 eV BE. After reduction with hydrogen, nickel oxide was mainly reduced to metallic nickel but about 30% of the nickel was still in the form of Ni^{2+}. The Ce^{4+} satellite practically disappeared indicating the reduction of Ce^{4+} The Ni/Zr atomic ratio, measured by XPS decreased from 0.098 to 0.059 and the surface carbon concentration decreased from 29.4 at.% to 6.2 at.%. We should note that by re-oxidation at room temperature with air, the initial Ni/Zr ratio was restored. This increase in the Ni/Zr ratio at room temperature is an indication of the mobility of nickel in the catalyst. $CO_2 + CH_4$ reaction at 660 °C had no influence on the shape of Ni, Ce and Zr spectra but carbon peak broadened and shifted to lower BE (see Fig. 13(2)(c)). At the same time there was a decrease of about 4 eV in the charging of the sample, indicating an increased conductivity of the sample due to the carbonaceous layer. The "as prepared" state but with negligible amount of carbon could be regenerated by treating in air at 700 °C (13(2)(d)). A second $CO_2 + CH_4$ reaction returned the catalyst into the state as it was after the first reaction (13(2)(c) and 13(2)(e)). This suggests that the state of the catalyst adopts itself to the reaction conditions independent of the state (oxidized or reduced) before the reaction. XPS data of a catalyst used ex situ for a long time in the catalytic tests are listed in the last line in Table 2. The increased carbon concentration is the major difference compared to the in situ reactions.

Finally in order to elucidate the surface elementary processes, methane decomposition without CO_2 was studied on the oxidized $NiCe_{0.6}Zr_{2.97}$ (sg) sample. In Fig. 14(a) the products of methane conversion are plotted vs. temperature. Up to 470 °C no products are formed, while about CO and water are measured by QMS together in a 30 °C gap. Since there is no oxygen source present in the gas phase, most likely some amount of oxygen is taken from the easily removable oxygen in cerium oxide, since the sample was oxidized before the experiment. At higher temperature only hydrogen is formed from methane leaving carbonaceous deposit on the sur-

Table 2
Surface concentrations of $NiCe_{0.6}Zr_{2.97}$ (sg) and charging values determined by XPS.

Treatment[a]	O (%)	C (%)	Ni (%)	Zr (%)	Ce (%)	Ni/Zr	Charging (eV)
As prepared	50.5	29.4	1.55	15.8	2.8	0.098	5.1
H_2 at 770 °C	59.9	6.2	1.11	18.8	2.8	0.059	4.1
Reaction in 30% CO_2 + 70% CH_4 at 660 °C	40.7	28.5	0.58	14.4	2.6	0.04	1.0
air at 700 °C	66.8	5.06	2.93	20.7	4.4	0.14	4.1
Reaction in 30% CO_2 + 70% CH_4 at 660 °C	43.8	38.6	0.28	14.9	2.4	0.019	2.0
Ex situ catalytic test	41.3	47	0.4	9.4	2.3	0.04	1.2

[a] In the sequence of in situ treatments.

face. As shown in Fig. 14(b), this carbon can be easily removed by O_2 at around 400 °C in the form of CO_2. After the second reaction the carbon removal with CO_2 starts at 600 °C and only CO is formed most likely by reverse Boudouard reaction (Fig. 14(c)). Józwiak et al. studying $NiRh/SiO_2$ detected graphitic carbon formation (by XRD) but the catalyst was active and stable. This carbon could be partially gasified by CO_2, although the subsequent TPO removed the remaining carbon from the catalyst [36]. In our case after CO_2 treatment, the TPO with O_2 (not shown in Fig. 14. as the last step) could not remove further coke from the sample, thus, all the carbon deposit was removed by CO_2, probably by the aid of mixed oxide support in activating CO_2.

4. Conclusions

Ce–Zr-oxide supported monometallic Ni and bimetallic NiRh and NiCo catalysts were prepared by pseudo sol–gel method based on thermal decomposition of metallic propionates. Impregnated catalyst on the same type of support ($Ce_2Zr_2O_8$ prepared by sol–gel) was synthesized as a reference. The as prepared support was face-centered cubic structure of $Ce_{0.6}Zr_{0.4}O_2$. It was stated that a part of Ni was inside the fluorite structure and the other one was rejected. No diffraction patterns corresponding to cobalt or rhodium oxides were observed.

Catalytic tests were carried out with ($CH_4/CO_2/Ar = 10/10/80$) and without diluting gas ($CH_4/CO_2 = 70/30$) demonstrated that the most active sample was the $NiRhCe_2Zr_{1.51}$ (sg). The original activity could be regained for all the samples by calcinations/reduction treatment. Co and the Rh containing bimetallic sample seemed to be stable catalyst, the impregnated Ni catalyst only slightly, while sol–gel prepared Ni samples slowly but surely deactivated during the long term run. Due to methane dry reforming and high temperature oxidation/reduction treatments, support degradation and segregation happened, sintered metal particles were removed from the support by the growing carbonaceous filaments and surrounded by network of nanotubes, encapsulated by graphitic layer, but there was a certain amount of Ni in strong interaction with the support probably still included in the oxide matrix.

TPO results demonstrate that there is no straightforward relation between catalytic activity and amount of surface carbon. This indicates that carbon contamination may play a dynamic role in dry reforming reaction to produce CO. Thus, the deactivation process can be caused partially by the re-oxidation of Ni into NiO during the reaction and partially by detrimental coke formation.

XPS measurements and catalytic reaction only after oxidation suggested that the state of the catalyst adopts itself to the reaction conditions and is independent of the state (oxidized or reduced) before the reaction. When pure methane was decomposed on Ni prepared by sol–gel method, the carbonaceous deposit could completely be removed by the subsequent CO_2 treatment, emphasizing the active role of Ce–Zr mixed oxide support in gasification of surface coke.

Acknowledgements

The authors are thankful for the support from ERACHEMISTRY (grant # NN75009). The authors are greatly indebted to Zoltán Schay for XPS measurements.

References

[1] L. Guczi, G. Stefler, O. Geszti, I. Sajó, Z. Pászti, A. Tompos, Z. Schay, Appl. Catal. 375 (2010) 236–246.
[2] A.R.S. Darujati, W.J. Thomson, Chem. Eng. Sci. 61 (2006) 4309.
[3] N.A. Pechimuthu, K.K. Pant, S.C. Dhingra, Ind. Eng. Chem. Res. 46 (2007) 1731–1736.
[4] F. Pompeo, N.N. Nichio, A.A. Ferretti, D. Resasco, Int. J. Hydrogen Energy 30 (2005) 1399–1405.
[5] S. Therdthianwong, A. Therdthianwong, Ch. Siangchin, S. Yongprapat, J. Hydrogen Energy 33 (2008) 991–999.
[6] M. Rezaei, S.M. Alavi, S. Sahebdelfar, Liu Xinmei, Ling Quian, Zi-Feng Yan, Energy Fuel 21 (2007) 581–589.
[7] M. Rezaei, S.M. Alavi, S. Sahebdelfar, X. Liu, P. Bai, Z.-F. Yan, Appl. Catal. B 77 (2008) 346–364.
[8] M. Rezaei, S.M. Alavi, S. Sahebdelfar, Z.-F. Yan, Mater. Lett. 61 (2007) 2628–2631.
[9] V.R. Choudary, K.C. Mondal, T.V. Choudary, Appl. Catal. A 306 (2006) 45–50.
[10] S. Corthals, J. Van Nederkassel, J. Geboers, H. De Winne, J. Van Noyen, B. Moens, B. Sels, P. Jacobs, Catal. Today 138 (2008) 28–32.
[11] C.E. Daza, C.R. Cabrera, S. Moreno, R. Molina, Appl. Catal. A 378 (2010) 125–133.
[12] C.E. Daza, J. Gallego, F. Mondragón, S. Moreno, R. Molina, Fuel 89 (2010) 592–603.
[13] J.A. Montoya, E. Romero-Pascual, C. Gimon, P. Del Angel, A. Monzón, Catal. Today 63 (2000) 71–85.
[14] J.C. Vargas, E. Vanhaecke, A.C. Roger, A. Kiennemann, Stud. Surf. Sci. Catal. 147 (2004) 115–120.
[15] F. Romero-Sarria, J.C. Vargas, A.C. Roger, A. Kiennemann, Catal. Today 133–135 (2008) 149–153.
[16] E. Ambroise, Ph.D thesis, Strasbourg 2010.
[17] M.C.J. Bradford, M.A. Vannice, Catal. Rev. Sci. Eng. 41 (1999) 1.
[18] M.R. Goldwasser, M.E. Rivas, E. Pietri, M.J. Pérez-Zurita, M.L. Cubeiro, L. /Gingembre, L. Leclercq, G. Leclercq, Appl. Catal. A 255 (2003) 45–57.
[19] Gustavo Valderrama, A. Kiennemann, M.R. Goldwasser, Catal. Today 133–135 (2008) 142–148.
[20] German Sierra Gallego, Catherine Batiot-Dupeyrat, Joel Barrault, Elizabeth Florez, Fanor Mondragon, Appl. Catal. A 334 (2008) 251–258.
[21] D. Chen, R. Lodeng, A. Anundskas, O. Olsvik, A. Holmen, Chem. Eng. Sci. 56 (2001) 1371–1379.
[22] V.A. Tsipouriari, A.M. Efstathiou, X.E. Verykios, J. Catal. 161 (1996) 31–42.
[23] M.A. Goula, A.A. Lemonidou, A.M. Efstathiou, J. Catal. 161 (1996) 626–640.
[24] X. Junke, Z. Wei, W. Jihui, L. Zhaojing, M. Jianxin, Chin. J. Catal. 30 (11) (2009) 1076–1084.
[25] J.W. Snoeck, G.F. Froment, M. Fowles, J. Catal. 169 (1997) 240–249.
[26] L.A. Avdeeva, T.V. Reshetenko, V.B. Fenelonov, A.L. Chuvilin, Z.R. Ismagilov, Carbon 42 (2004) 2501–2507.
[27] B. Koubaissy, A. Pietraszek, A.C. Roger, A. Kiennemann, Catal. Today, doi:10.1016/j.cattod.2010.01.050.
[28] D. San-José Alonso, J. Juan-Juan, M.J. Illán-Gomez, M.C. Román-Martínez, Appl. Catal. A: Gen. 371 (2009) 54–59.
[29] W. Pan, Ch. Song, Catal. Today 148 (2009) 232–242.
[30] W. Gac, A. Denis, T. Borowiecki, L. Kepinski, Appl. Catal. A: Gen. 357 (2009) 236–243.
[31] G. Carneiro de Araujo, S. Maria de Lima, J.M. Assaf, M.A. Pena, J.L. Garcia Fierro, M. do Carmo Rangel, Catal. Today 133–135 (2008) 129–135.
[32] Y. Zhang, K.J. Smith, J. Catal. 231 (2005) 354–364.
[33] M. Matsukata, T. Matsushita, K. Ueyama, Chem. Eng. Sci. 51 (1996) 2769–2774.
[34] F. Frusteri, L. Sparado, F. Arena, A. Chuvilin, Carbon 40 (2002) 1063–1070.
[35] X. Zhu, P. Huo, Y. Zhang, D. Cheng, C. Liu, Appl. Catal. B: Environ. 81 (2008) 132–140.
[36] W.K. Józwiak, M. Nowosielska, J. Rynkowski, Appl. Catal. A: Gen. 280 (2005) 233–244.